Simulation and Optimization of Variable Ethylene Production from Carbon Dioxide Utilizing Intermittent Electricity

Jakob Hoch [a], Daniel Schicksnus [a]

[a] *Aachener Verfahrenstechnik - Process Systems Engineering, RWTH Aachen University, Aachen, Germany*

June 2025

Abstract

Ethylene is a key platform chemical in global manufacturing, yet its conventional production via steam cracking is highly energy-intensive and a major source of industrial CO_2 emissions. This study proposes a sustainable alternative for ethylene synthesis through the electrochemical reduction of captured CO_2 via alkaline electrolysis powered by intermittent offshore wind energy. A selective catalytic pathway for the CO_2 reduction reaction is identified and modeled in ASPEN PLUS®, with full integration of reaction, separation, and recycle units. To address the variability in renewable energy supply, a time-variable process optimization framework is developed in Pyomo, enabling operational flexibility through integrated process planning and scheduling. Three electricity sourcing scenarios are analyzed, each representing different balances between grid and renewable power. A gate-to-gate life cycle assessment reveals a significant greenhouse gas emission reduction, with the most renewable-intensive configuration achieving net-negative emissions of $-2.4\ kg_{CO_2}$ per kg ethylene produced. This represents a substantial improvement over conventional fossil-based processes and a notable reduction compared to the state of research on CO_2-based processes, demonstrating the potential for de-fossilizing ethylene production on a large scale. The break-even ethylene price is calculated at 6.06 € per kg, and the required carbon certificate price is 1,770 € per ton. While the process is not currently cost-competitive, it shows significant potential for viability given technological cost reductions and future market or policy conditions. These findings highlight the technical feasibility and environmental advantages of renewable-powered, CO_2-to-ethylene conversion, offering a promising pathway for decarbonizing ethylene production and reducing fossil dependency in the chemical sector.

1. Introduction

The primary objective of the Paris Climate Agreement is to ensure that global warming remains below 1.5 °C compared to the preindustrial average [1]. However, the World Meteorological Organization reported that the global temperature was already above this threshold for the first time in 2024 [2]. Therefore, it is more important than ever to reduce greenhouse gas emissions. One way to reduce emissions in processes that cannot be easily converted to low carbon alternatives is by capturing carbon-dioxide (CO_2) in the flue gas stream [3]. This captured CO_2 can be stored or reduced to other chemicals. To reduce CO_2 into chemicals, electrocatalysis can be used. Recently, various articles have reported catalysts that allow CO_2 to be directly reduced to C^{2+}-products, especially ethanol and ethylene [4, 5, 6]. Ethylene is one of the most important petrochemical products and is used in the production of polymers (e.g. PE, PET, PVC) and various industrial chemicals [7]. Producing ethylene at competitive prices and in large quantities without relying on fossil carbon therefore is a major step in de-fossilizing the chemical industry. However, the reduction of CO_2 is an energy-intensive process [8]. Therefore, it should be supplied with energy from renewable sources. With the intermittent availability of these renewable sources, processes must be optimized for flexible operation to reap the full benefits of changing electrical supply.

In this work, we first compare different catalytic processes that convert carbon-dioxide into ethylene and choose the reaction pathway that shows the most promising results. We then analyze various separation options and model the resulting process with integrated reaction, separation, and recycling that produces high-purity ethylene from CO_2 feedstock in ASPEN PLUS® [9]. After this, we perform a heat integration, propose an incorporation of the process into the Belgian chemical network, and choose a source of renewable energy. Next, we perform a time variable integrated process planning and scheduling (IPPS) [10, 11, 12] optimization of the plant.

The optimization follows the availability of renewable energy, determining the optimal design capacity for the

Table 1: Summary of Electrocatalyst Performance

Catalyst	**Max C_2H_4 FE [%]**	**Full Cell EE [%]**	**CD $[\frac{mA}{cm^2}]$**	**Electrolyte**
Cu-12 Oligomer [13]	72.0	20.0	230	Water
CuO-SH [14]	76.9	N/A	340	0.1 M $KHCO_3$
Cu Polyamine [15]	87.0	50.0	35	10 M KOH
F-Cu [16]	69.5	37.0	100	0.05 M KOH
CuO Nanoplate [17]	74.8	27.6	200	0.5 M KCl
Cu Nanosheets [18]	83.4	N/A	60	1 M K_2SO_4
CuO/Al_2CuO_4 [6]	82.4	N/A	42	0.1 M $KHCO_3$
Stepped Cu surface [19]	77.4	N/A	17	0.1 M $KHCO_3$

electrolysis cell and intermediate storage tanks, as well as the corresponding operation strategy. Finally, we determine key performance indicators and assess the economic and ecological feasibility of the process. We further compare the results with a recent study by Kim and Benavides [20].

2. Choice of Key Chemical and Systematic Screening of Reaction and Process Pathways

In the following section, we explain the choice of our key chemical product: ethylene. Then, we systematically screen for different reaction pathways that produce ethylene from CO_2. Finally, we compare the separation pathways to produce high-purity ethylene.

2.1. Choice of Key Chemical

Carbon dioxide removed from the atmosphere or captured from flue gas needs to be processed to make sure it does not leak back into the atmosphere. An option discussed is to store CO_2 in former natural gas sites or by mineral carbonation [21]. Another is to reduce CO_2 into value-added chemicals through biochemical and catalytic processes [8]. One particularly promising approach is electrochemical reduction because it can use a renewable electricity supply [22]. Electrocatalysts have been developed to reduce CO_2 into CO-syngas [23], methanol [24], and formic acid [25], among others.

Recently, more research focused on methods that convert CO_2 into C^{2+}-products, especially ethanol and ethylene [26, 13, 27]. Ethylene is one of the most important petrochemical products with a production of 329 Million Tonnes in 2024 and projected to grow to over 400 Million Tonnes per year in 2030 [28]. Therefore, establishing pathways that can produce ethylene without the use of fossil carbon sources is imperative in the shift towards a more sustainable chemical industry.

For these reasons, we focus on developing a novel process that incorporates renewable electricity to convert CO_2 into a stream of high-purity ethylene.

2.2. Screening of Reaction Pathways

To choose a reaction that reduces CO_2 to ethylene, we systematically screen a large number of different reaction pathways that were experimentally verified and reported in scientific journals. Recently, several studies have focused on reducing CO_2 to C^{2+}-products in multiple stages [29, 30]. However, these pathways result in a more complicated and more expensive process configuration due to more reactors and a potential need for additional separation processes between reactors [30]. Therefore, we focus on assessing the performance of different direct reduction reactions.

In Table 1 a selection of carbon-dioxide reduction reaction (CO_2RR) is shown that directly reduce CO_2 to ethylene. They are compared by the maximum ethylene faradaic efficiency (FE), the efficiency with which electrons are transferred in a chemical reaction, the full cell electrical efficiency (EE), the percentage of electrical energy not lost as heat, current density (CD), the current flowing through an area of the electrode, and the electrolyte used. All reactions were tested in laboratory scale with electrolytic flow cells by the respective groups after a design by Ma et al. [5]. The two components we consider to be most important are the ethylene FE and the EE. With the electricity demand of CO_2RR being the largest driver of energy demand (see Section 4.5), this is especially important. In both regards, the Polyamine-incorporated Copper catalyst [15] shows superior performance compared to the other reactions cataloged. However, it does show a lower current density compared to most other reactions. This increases the capital expenditure for the electrolysis. A report on the capital cost of hydrogen electrolysis cells by Fraunhofer-Gesellschaft [31] finds that the installed cost of an electrolysis system is dominated by costs not directly related to the cells. Therefore, we assume this factor to be of less importance and choose the Polyamine-incorporated Copper catalyst [15] for our reaction.

The catalyst was tested inside an alkaline flow cell as described by Ma et al. [5]. The flow cell has three in-

put streams: one gaseous stream of CO_2 and two electrolyte streams separated by an anion exchange membrane (AEM). The gaseous products remain inside the gas stream while liquid products dissolve into the electrolyte stream. All oxygen diffuses through the AEM and exits on the anode side.

Table 2: Faradaic Efficiencies of Electrocatalytic Reaction

Product	**Faradaic Efficiency** [%]
Ethylene C_2H_4	87.0
Ethanol C_2H_5OH	5.5
Carbon monoxide CO	5.5
Hydrogen H_2	2.0

The catalyst synthesized by Chen et al. [15] features a FE of 87% for ethylene in a 10 M potassium hydroxide (KOH) electrolyte, which is, to the best of the authors knowledge, the highest value reported for any direct electrocatalytic CO_2 to ethylene reduction. The reaction also produces a number of side products. The largest of them are shown in Table 2. We disregard all side products with FEs under 1% for our analysis of the process.

Most of the articles on laboratory scale experiments do not report their findings on maximum single-pass conversion. However, Ma et al. [16] conducted similar alkaline flow-cell electrocatalytic reduction experiments with a different copper catalyst and found a single-pass conversion of 16.5% which we assume for our reaction as well. We further assume that the reaction can be developed to reach the lab-scale FE, EE, and conversion on an industrial scale by the time our process is implemented.

2.3. Screening of Separation Pathways

The low single-pass conversion to ethylene, together with the production of side products and inclusion of impurities from the CO_2-feed (see Section 3.1) mean that the gaseous product stream must be separated and purified before it can be sold. Today, most ethylene is produced by steam cracking, which produces mostly other C_2-hydrocarbons as side products [32]. The classic separation method to produce high purity ethylene from the product is through cryogenic distillation [33]. Recently, many studies focused on more energy-efficient separation of ethylene from ethane and acetylene [34, 35, 36] to purify ethylene from steam cracking processes.

However, our product does not contain large amounts of C_2-hydrocarbons. Instead, it consists mainly of unreacted CO_2 with the other major impurities being CO and H_2. Although some studies have focused on the removal of CO_2 by adsorption from an ethylene stream [37, 38], these methods are designed to remove small fractions of CO_2, not separate a stream where CO_2 is the main component.

Therefore, we select to separate the product via a two-stage cryogenic distillation setup. The first distillation separates CO_2 from the product stream and produces a bottom stream that is recycled back to the electrolysis cell. Since CO_2 is the heaviest component, it can be purified here. This distillation column is operated at increased pressure because it increases the temperature, which allows the condenser to be cooled via a single-stage refrigeration cycle. This significantly reduces its electricity demand and cost. The distillate stream is then fed into a second distillation column in which ethylene at 99.9 *mole*% purity is separated as the bottom stream. This distillation runs at an even lower temperature and therefore requires liquid nitrogen (LN2) for condenser cooling.

The liquid electrolyte stream that exits the reactor contains dissolved ethanol, the only liquid product produced in the electrocatalytic reaction. The separation of ethanol and water is complicated by a vapor-liquid azeotrope at 91 *mole*% ethanol [39]. Therefore, we enrich the ethanol to a purity of at least 82 *mole*% using an ambient pressure distillation column and burn the stream for heat credit. Due to its much higher boiling point [40], KOH can be assumed as a non-volatile component and ends up in the bottom stream that is recycled back into the electrolysis cell.

3. Integration in Belgian Electrical and Chemical Networks

In the following section, we outline how our process integrates into Belgium's network of renewable electricity and chemical production. First, we choose a source of carbon dioxide and a destination for the ethylene produced. We then choose a source of renewable energy and, based on the choices before, a location for the chemical plant.

3.1. Source of Carbon Dioxide

The most important feedstock of our process is CO_2. In 2023, Belgium emitted 106.5 million Tonnes of CO_2-equivalents [41]. Of these emissions, 27% can be attributed to industry [41]. Industrial emissions are a preferred subject for carbon capture because they produce flue gas streams with large amounts of CO_2 at a high concentration. Currently, this is the cheaper option compared to direct air capture (DAC) [42].

To collect CO_2 from various industrial sources and distribute it to potential storage and utilization sites, Fluxys proposed to build a CO_2-pipeline [43]. The pipeline will run through most of Belgium and parts of Germany's Rhine-Ruhr region. Several major terminals are suggested

to be constructed in Antwerp, Ghent, Liège, and Zeebrugge. Using this pipeline, we assume to have access to a constant stream of CO_2 with reliable quality.

Fluxys published a proposal for the carbon specification in their pipeline. Using this specification, we add several contaminants to the stream of CO_2 that we include in the process synthesis (shown in Table 3) [44].

Table 3: Composition of CO_2 feed stream

Chemical	**Mole fraction** [%]
Carbon dioxide CO_2	95.5
Nitrogen N_2	2.40
Methane CH_4	1.00
Hydrogen H_2	0.750
Argon Ar	0.400
Carbon monoxide CO	0.0750
Water H_2O	0.00400
Oxygen O_2	0.00400

We add these impurities to optimize the process for the worst possible case. Therefore, with a higher purity CO_2 feed the process will also produce ethylene with the required specification. Special attention should be paid to the contaminant methane, as it is also a hydrocarbon. The similar thermodynamic properties of methane and ethylene increase the difficulty of separation.

We assume zero cost for the CO_2 stream as it is a waste product from other processes, neglecting the costs associated with pipeline transportation. Instead, we assume to generate revenue by selling certificates for CO_2 removed from the atmosphere through the EU emissions trading system (ETS) [45]. However, the market for CO_2 certificates is volatile and the price of future certificates is uncertain. For our analysis, we choose a constant certificate price adapted from the predictions for CO_2 pricing in Belgium in the 2030s at 100 €/Tonne [46].

3.2. Destination of Ethylene

The ethylene produced is assumed to be sold to a pipeline operated by ARG. This pipeline connects ethylene producers and consumers in Belgium and the Rhine-Ruhr region in Germany [47]. It has several terminals, including one connecting it to a BASF plant in Antwerp that produces and consumes ethylene [48]. To ensure high-quality products, the pipeline requires a minimum purity of ethylene of 99.9 *mole*% [49]. The sales price of ethylene is assumed to be 827 €/tonne corresponding to the market price in Europe [50].

3.3. Source of Renewable Electricity

CO_2 reduction reactions are an energy-intensive process [51], which requires careful consideration of the source of this energy. Currently, Belgium's energy mix is still dominated by fossil sources, such as natural gas and nuclear power [52]. However, in recent years, there has been a significant increase in renewable electricity generation, of which wind power contributed the largest share [52]. Belgium's location on the North Sea makes it a prime location to install large offshore wind parks. More than 2 GW of capacity have already been installed in Belgium's first offshore wind zone [53].

A second offshore wind zone is under construction in Belgium's exclusive economic zone (EEZ) southwest of the first area. In its center, it features the first artificial island built to channel and distribute the electricity produced by wind turbines [54]. The first lot that is developed in this zone has a capacity of 700 MW and is scheduled to be completed by 2030 [55]. Up to 50 % of the capacity of the plant can be sold directly to customers through a power purchase agreement (PPA) [56]. A PPA is a long-term contract for the sale of electricity that usually states an amount of electricity purchased and a fixed price contract. Therefore, the market risk is reduced for both parties [57]. We assume that we buy electricity at a maximum of 350 MW through a PPA at a price of 87.43 €/MWh. The price is comparable to the levelized electricity cost for similar offshore wind projects already operational in Belgium [58].

3.4. Choice of Location

Antwerp is the location of large terminals for both the CO_2 as well as the ethylene pipelines. It is also close to the North Sea, where offshore wind parks are being built. Furthermore, the largest chemical industry production cluster in Belgium is located in the port of Antwerp-Bruges. There, several large chemical companies have constructed major production sites [59]. This gives us the opportunity to benefit from existing infrastructure in addition to the pipelines mentioned above. Therefore, we choose the port of Antwerp-Bruges as the proposed plant location for our process.

4. Design and Simulation of Integrated Plant

The following section first clarifies the design of our overall plant and the tools used to synthesize and simulate it. Then, it focuses more closely on key design decisions and optimization of parameters in each part of the process. Finally, it explains the integration of the heat network and the electric utility.

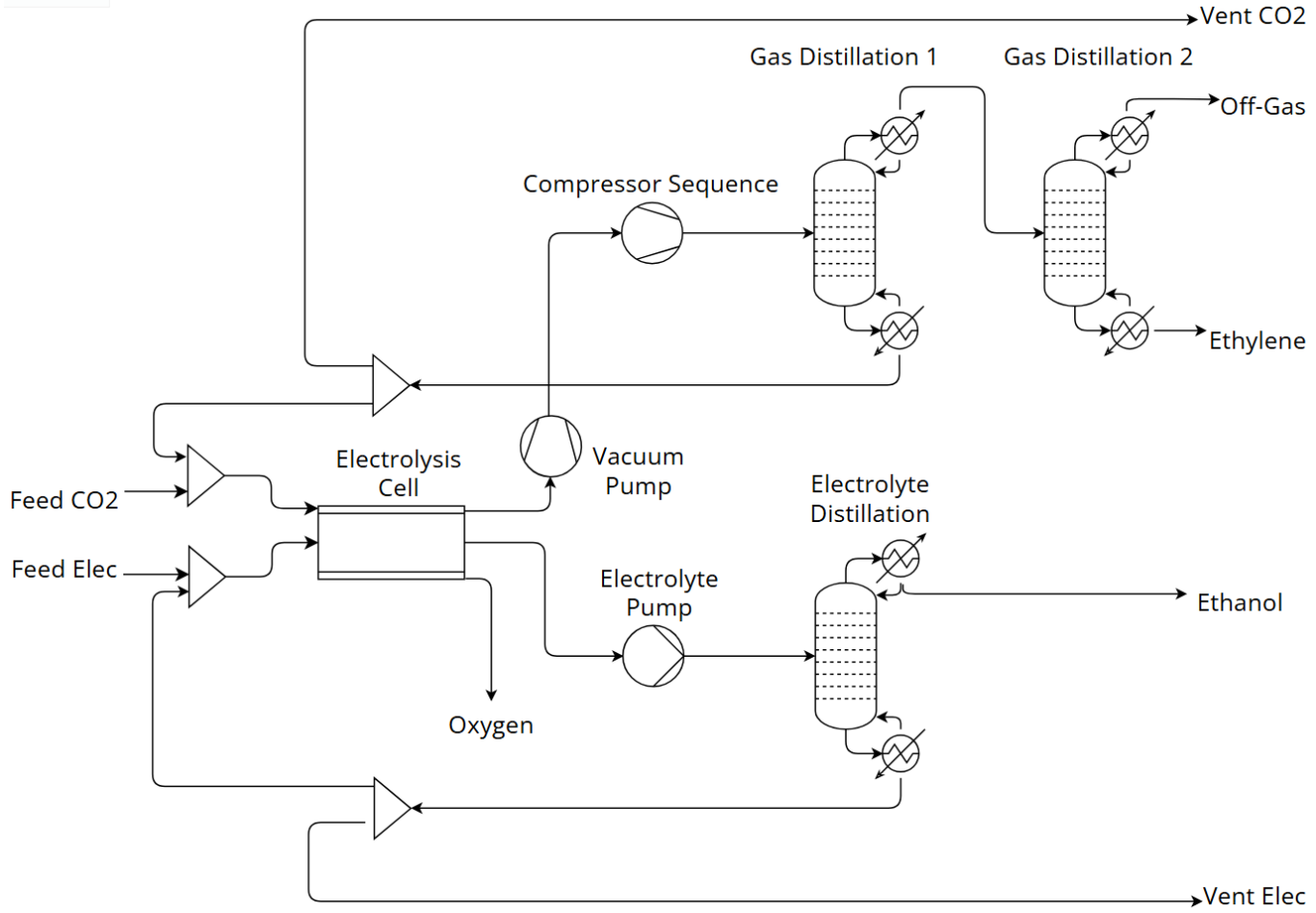

Figure 1: Simplified process flow diagram of the CO_2 reduction and separation process without valves and heat exchanger network

4.1. Overall Plant Design

To simulate the conversion of CO_2 to high purity ethylene, we synthesize the entire process including recycle streams in ASPEN PLUS® [9]. The process, we use the *NRTL* thermodynamic model. A simplified process flowsheet, excluding heat exchangers and valves, of the process as synthesized in ASPEN can be found in Figure 1. The process can be divided into three main parts: The electrocatalytic reduction reaction, the separation of the gaseous products, and the separation of the electrolyte stream. These parts are specified in the following sections.

4.2. Electrocatalytic Reduction Reaction

The central operation in our process is the carbon dioxide reduction reaction. The specifics of the reaction are described in Section 2.2. The reaction has two feed streams: the CO_2 stream and the 10 *M KOH* electrolyte stream. Both streams are combined from material added to the process from the outside and material recycled back from the separation processes. To model the electrolysis cell using ASPEN, we divide the reaction into three unit operation models. The first one is an *RSTOIC* that models the following four reactions:

$$2\,CO_2 + 2\,H_2O \rightleftharpoons C_2H_4 + 3\,O_2 \quad (1)$$

$$2\,CO_2 \rightleftharpoons 2\,CO + O_2 \quad (2)$$

$$2\,H_2O \rightleftharpoons 2\,H_2 + O_2 \quad (3)$$

$$2\,CO_2 + 3\,H_2O \rightleftharpoons C_2H_5OH + 3.5\,O_2 \quad (4)$$

The reactor uses a fixed conversion method that takes into account FE, electron transfer in each reaction, and overall conversion (the calculations can be found in the **Supplementary Information**).

The *RSTOIC* returns a combined stream of all products that must be separated to model electrolysis accu-

rately using an idealized separation model. This unit separates the product into three streams:

- Gaseous products and unreacted carbon dioxide (CO_2, C_2H_4, H_2, CO, CH_4, Ar, and N_2)
- Electrolyte and dissolved ethanol (H_2O, KOH, and C_2H_5OH)
- Oxygen that diffused through the anion exchange membrane (O_2)

The gaseous product stream then passes through a vacuum pump, modeled as a compressor, because the electrolysis cell is held at 0.8 *bar* to allow all gaseous products to escape into the gas stream [16].

4.3. Gas Separation

The gaseous stream contains a number of different materials that must be removed from the stream to produce ethylene that satisfies the purity requirement. Furthermore, most CO_2 must be recycled back into the electrolysis cell to increase the utilization of CO_2. To achieve this, we include two cryogenic distillation columns that are simulated in ASPEN using the *RADFRAC* model.

The first column removes CO_2 from the mixture under high pressure. Separation of CO_2 and ethylene, the second heaviest component in the mixture, is a difficult process due to close boiling points of the two components. To limit the capital expenses (CAPEX) of the distillation column, we restrict the number of trays to 150 and include a partial condenser that allows light gases to escape the column. To be able to condense the other gases using a single-stage refrigeration cycle with an approach temperature of 8 $°C$ [60], the condenser temperature is restricted to be above -35 $°C$. This leads to a condenser pressure of 36.5 *bar* which is achieved using a three-stage compressor with intercoolers.

This column is by far the largest contributor to both the capital and the operational expenses of the separation process. Therefore, it should be optimized to reduce investment and utility costs. To reduce the refrigeration duty, the distillation column must have the lowest possible reflux ratio that still achieves the required product quality after the second column. We optimize the reflux ratio in the completed process including separation and recycling streams. The minimum reflux ratio needed is $R = 96$, which is the main reason the column has a condenser duty of 51 MW.

The second distillation separates ethylene from all other contaminants, especially methane, and produces a stream of the required purity. It operates at a lower pressure of 15 *bar* to reduce the separation effort. However, the partial condenser operates at a temperature of -130 $°C$, necessitating the use of LN2 as a refrigerant. The condenser duty is 1.5 MW at a reflux ratio of 3.5 in a column with 8 trays. The off-gas from the condenser contains several flammable components. It is therefore burnt as a heat source with the energy sold to other chemical plants.

4.4. Electrolyte Separation

The electrolyte exiting the electrolysis cell has a small amount of ethanol dissolved in it. Before it can be recycled, the ethanol must be removed from the stream. This is done using an ambient-pressure distillation column. The column is modeled as $RADFRAC$ with a total condenser with a reflux ratio of 6, and consists of 40 trays. The distillate has a purity of 83 $mole\%$ ethanol, which is significantly below the azeotrope. The ethanol is burnt as a heat source and the excess heat is sold to other plants.

4.5. Heat Integration and Electric Refrigeration

To function, our process needs a number of different utilities: electricity, low-pressure steam, cooling water (both for cooling hot streams and heating streams below ambient temperature), refrigerant, and LN2. In total, the process needs 106 MW electricity, 51 MW heating, and 115 MW cooling. The specific total energy required in this configuration is 260 $MJ/kg_{ethylene}$.

To reduce the energy demand and therefore the cost of production, we perform a heat integration. We carry out a pinch analysis using a tool by TLK Energy [61]. This reduces the heating demand to 1 MW and the cooling demand to 65 MW with a total of 50 MW of heat recovered in the process.

After heat integration, the 51 MW refrigeration duty in gas separation and the 1.5 MW LN2 duty remain. Using the coefficient of performance (COP) for refrigeration, they are converted to equivalent electricity duties (see **Supplementary Information**). Furthermore, the heat duty that remains is generated by burning a part of the ethanol stream produced on-site to generate the equivalent amount of low-pressure steam.

After heat integration, the process needs 124 MW electricity and 12 MW cooling water in steady state operation. The specific total energy demand is reduced to 192 $MJ/kg_{ethylene}$, a reduction by 26 % compared to the unintegrated process.

5. Process Optimization under Intermittent Renewable Energy Supply

One of the main aspects of our process is the integration of renewable intermittent energy. Intermittent renewable energy sources, such as solar and wind, present significant challenges to process industries because of their

variability. As discussed in Section 3.3, we choose to use off-shore wind energy produced in the Princess Elizabeth zone in the North Sea. To maintain efficient and reliable chemical production, we use time variable IPPS optimization strategies [10, 11, 12]. This section describes the methodologies used to integrate intermittent renewable energy, formulates the optimization model, and illustrates the optimization results of three different scenarios of electricity use in a case study.

5.1. Renewable Energy Integration

Renewable energy has obvious benefits for the sustainability of our process, yet it also introduces challenges related to its volatile nature. In our design, we focus on wind electricity from an offshore installation in the Princess Elizabeth zone as the sole renewable energy source. However, the inherent fluctuations in wind intensity necessitate additional strategies to ensure continuous and optimal process operation. Possible approaches include:

- **Energy Storage Systems:** [62] Batteries, thermal storage, and other storage technologies can buffer energy supply fluctuations. Although storage systems on the scale required for our process remain economically unfeasible at present [63, 64], they are an important consideration for future integration.
- **Hybrid Energy Systems:** [65] The combination of multiple renewable sources, such as wind and solar, can smooth out overall variability due to complementary generation profiles. Additionally, non-renewable source scan also be included to balance the intermittency of renewable sources. For our current design, we focus solely on wind electricity as our renewable source and include grid electricity as a backup source.
- **Real-Time Monitoring:** [66] The implementation of sensors and advanced metering infrastructure allows for continuous data acquisition. This enables adaptive control strategies that optimize energy usage, ensuring that the process can respond immediately to changes in wind energy generation.
- **Demand-Side Management:** [67] By adjusting process operations to coincide with periods of high renewable energy availability, we can maximize the utility provided by the renewable source. This is achieved by dynamically scaling the production rate and thus the electricity demand of the process based on real-time energy availability.

In summary, while energy storage remains cost-prohibitive at the required scale, our process design leverages real-time monitoring and demand-side management to align production with the available wind electricity. This integration framework supports the dynamic nature of renewable energy, ensuring that process operations can adjust in real time to varying energy inputs, thereby enhancing both process stability and sustainability.

5.2. Optimization Model

In our process design, the electrolysis cell represents the most significant electricity load, whereas the separation process has a relatively minor load. We make a few assumptions to simplify the steady state process design into a model that can be used for time variable optimization.

We assume that the electrolysis cell can be scaled continuously between its rated maximum throughput and being shut off completely with fixed quasi steady state efficiency and product conversion ratios of the reaction that do not depend on the operational level or process dynamics. The justification for this assumption is that we design our electrolysis cell to be composed out of multiple smaller units that work in parallel, such that scaling the operational level of the entire cell involves shutting of some of the smaller units, while keeping the rest at their rated throughput. This assumption is also reflected in the capital cost, as the parallel approach will scale worse with the rated capacity compared to a large single cell.

The separation process includes multiple large unit operations. However the separation still has a significantly smaller capital expense and uses less energy compared to the electrolysis cell. Because of this we simplify the modeling by neglecting any dynamic effects of the separation by running the separation at its steady state operational level and focusing solely on the time variable operation of the electrolysis cell.

Accordingly, we decompose our steady-state process into two distinct operational segments: the electrolysis cell, with a time variable operational level, and the separation unit, which operates at the fixed steady state. To enable time variable operation, we introduce two storage tanks with associated compressors to buffer material flows between these segments. As the electrolyte solution is recycled it does not need to be stored. Thus we focus on the storage of the gaseous components of our streams. The time-variable optimization model is designed to coordinate process operations with the intermittent nature of renewable energy supply. The decision variables in our model are denoted by: $\theta = \{L(t), E_j(t), S_l(t), Cap_{S_l}, Cap_L\} \in \mathbb{R}_+$ where:

- $L(t)[MW]$: The operating load of the electrolysis cell over time, with an associated flow $F(t)[Tonne/h] \propto L(t)[MW]$
- $E_j(t)[MW]$: The amount of energy consumed over

time from each source $j \in G, W$ where G and W represent grid and wind electricity respectively

- $S_l(t)[Tonne]$: The amount stored over time in storage tank $l \in R, I$ where R and I represent the reactants tank before, and the intermediary tank after the the electrolysis cell

- $Cap_{S_l}[Tonne]$: The maximum storage capacity of storage tank l

- $Cap_L[MW]$: The maximum load capacity of the electrolysis cell

We use an hourly discretization on our reference year, transforming the continuous time interval $I_{Year} = [0, T]$ with $T = 8760$ hours into $n_t = 8759$ equidistant time points t_i, for $i = 0, \ldots, T$ with a timestep of $dt = 1$ hour. The objective of our optimization is to minimize the equivalent annual cost (EAC) [68] of the variable operations within our process:

$$\min_{\theta} \left(\frac{CAPEX}{A_{n,i_a}} + OPEX \right) \tag{5}$$

where the annuity factor A_{n,i_a} is defined as [68]:

$$A_{n,i_a} = \frac{1 - \frac{1}{(1+i_a)^n}}{i_a} \tag{6}$$

with i_a representing the annual interest rate (or cost of capital) and n the assumed plant life.

We compute the CAPEX for each variable module using the power law provided in Perry's Handbook [69]:

$$C_M = P_{M,base} \cdot (Cap_M)^{p_M} \tag{7}$$

where $P_{M,base}$ is the base price of the module, Cap_M is the capacity of the module, p_M is the exponent with which the cost scale with the capacity, and C_M is the cost of the scaled module. We then aggregate the total CAPEX as:

$$CAPEX = \sum_{M} C_M \tag{8}$$

Similarly, the operational expenses (OPEX) for each utility are computed as:

$$C_U = \sum_{t_i=0}^{t_i=T} P_U(t_i) \cdot D_U(t_i) \cdot dt \tag{9}$$

where $P_U(t_i)$ and $D_U(t_i)$ are the price and duty of the utility at time t_i, dt is the timestep, and C_U is the summed cost of the utility over the reference year. The total OPEX are then given by:

$$OPEX = \sum_{U} C_U \tag{10}$$

The module costs are calculated in ASPEN PLUS® [9] and the values of the costing parameters are shown in Table 4.

Table 4: Costing parameters

Parameter	**Value**	**Source**
p_{EC} Electrolysis cell exponent	0.8	[69]
p_S Storage exponent	0.6	[69]
p_C Compressor exponent	0.7	[69]
n Plant life	25 Years	Assumption
i Annual interest rate	0.05	Assumption

The cost of the electrolysis cell is estimated separately. Holst et al. [31] provide a cost forecast for different water electrolysis types and sizes. We use their cost forecast of a 100 MW alkaline electrolysis assembly for the year 2030. From their work, we adapt the cost of the electrolysis stack to account for the lower current density of the CO_2RR. Other stack assembly costs (e.g. power electronics and piping) are adopted without changes while costs for separation and compression as well as engineering are excluded.

The time variable IPPS optimization model is given as:

$$\min_{\theta} \left(\frac{CAPEX}{A_{n,i}} + OPEX \right) \tag{11a}$$

$$\text{s. t.} \quad L_S + L(t_i) = E_W(t_i) + E_G(t_i), \tag{11b}$$

$$E_W(t_i) \leq A_W(t_i), \tag{11c}$$

$$E_G(t_i) \leq \max(L_L - A_W(t_i), 0.0), \tag{11d}$$

$$S_{R,I}(t_i) \leq Cap_{S_{R,I}}, \tag{11e}$$

$$L(t_i) \leq Cap_L, \tag{11f}$$

$$\forall_{t_i=0\ldots T}$$

$$S_R(t_i + dt) = S_R(t_i) + dt \cdot (F_N - F(t_i)), \tag{11g}$$

$$S_I(t_i + dt) = S_I(t_i) + dt \cdot (F(t_i) - F_N), \tag{11h}$$

$$\forall_{t_i=0\ldots T-dt}$$

$$L_N \leq Cap_L, \tag{11i}$$

$$S_{R,I}(0) = 0.5 \cdot Cap_{S_{R,I}}, \tag{11j}$$

$$S_{R,I}(T) = 0.5 \cdot Cap_{S_{R,I}}, \tag{11k}$$

where:

- $L_S[MW]$: The base load of the separation process

- $A_W(t_i)[MW]$: The amount of wind energy availability at time t_i

- $F_N[Tonne/h]$, $L_N[MW]$: The nominal flow through and load of the electrolysis cell
- $L_L(t)[MW]$: The load limit that can be supplemented by grid electricity

The model incorporates several constraints to model the different chemical and physical relations of our process. These include:

- **Mass and Energy Balances:** The energy balance (Equation 11b), includes the two electricity sources and the separation and electrolysis cell loads. The mass balances (Equations 11g and 11h) are enforced through an explicit Euler scheme [70], updating storage levels based on the net flows at each timestep.
- **Energy Source Variability:** Constraints account for the fluctuating supply of renewable wind electricity (Equation 11c) and limit the use of supplemental grid power (Equation 11d) to reduce CO_2 emissions.
- **Capacity Constraints:** The capacity of the electrolysis cell has to be high enough to produce the necessary amount of product (Equation 11i) and equal or exceed the load at every point in time (Equation 11f). Similarly, the storage capacity has to exceed the stored amounts at every point in time (Equation 11e).
- **Initial and Finishing Conditions:** The storage tanks have to be filled to half of their rated capacity in the beginning (Equation 11j) and end (Equation 11k) of the simulated timeframe.

The model is implemented in Python using the Pyomo optimization modeling framework [71, 72] and is solved using the IPOPT solver [73]. For the supplemental grid power we use real-world data on spot market energy prices $P_G(t_i)$ in Belgium [74, 75], adjusted such that the average energy price is the same as the average price paid by the Belgian industrial sector [76] after taxes and fees. Wind energy availability $A_W(t_i)$ data is provided by a simulation [77, 78, 79] of a wind park with an installed capacity of 350 MW. The simulation takes into account the location of the wind park, real world weather data for a given year, and the wind turbine type and height to simulate the electricity availability that can be provided by that park over the year. Our simulated wind park is located in the Princess Elizabeth zone as described in Section 3.3, and uses Siemens Gamesa SG 8.5-167 wind turbines which are similar to the ones recently used in existing Belgian wind parks [53]. The simulation is based on real world weather data from the MERRA-2 (global) dataset [80] capturing the fluctuations inherent in renewable energy supply. The cost of electricity from the windpark is fixed by the power purchase agreement as mentioned in Section 3.3. This integrated optimization framework enables real-time adjustments to process operations, ensuring optimal performance under variable energy inputs.

5.3. Case Study

The case study focuses on a chemical plant located in Belgium that utilizes captured CO_2 to synthesize ethylene. Given Belgium's climate, wind energy generation exhibits pronounced diurnal and seasonal fluctuations. To illustrate the application of the time variable optimization model, we consider three different operational scenarios:

- **Case 1: Static Grid Electricity (SGE)** In this baseline scenario, the plant relies exclusively on grid electricity, which is subject to varying market prices, while running the entire process at the designed steady state.

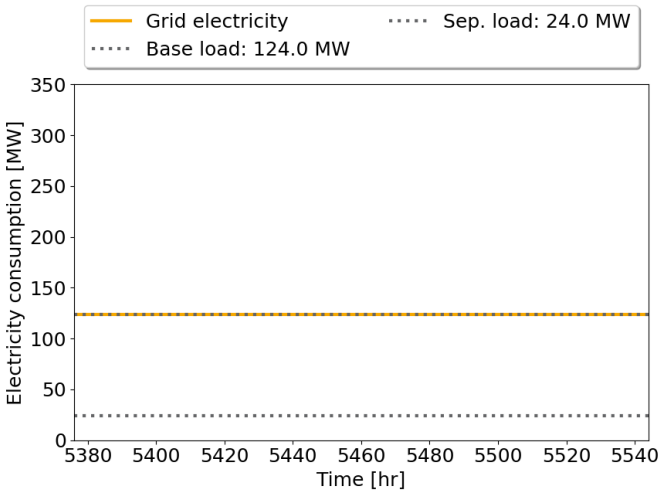

Figure 2: Electricity consumption over time for the SGE case

- **Case 2: Variable Wind Electricity (VWE)** In this scenario, the plant is integrated with wind electricity. The time variable optimization model can adjust the operational level of the electrolysis cell, and thus the storage levels, in our simulation in response to real-time renewable availability. The optimization is used to determine the optimal design of our variable process for the given real world data.

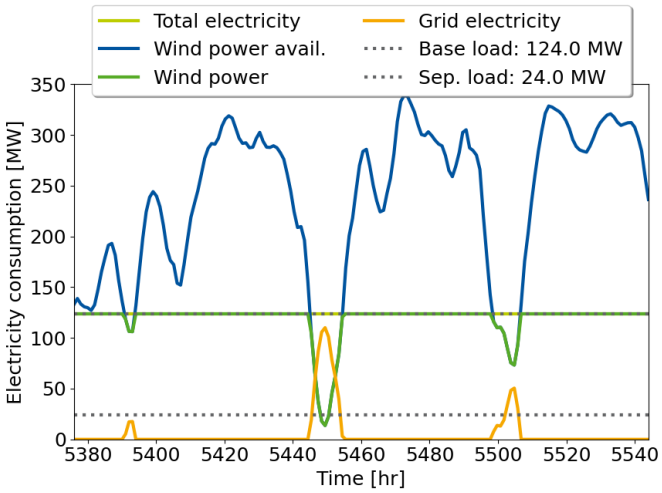

Figure 3: Electricity consumption over time for the VWE case

- **Case 3: Constrained Wind Electricity (CWE)** This scenario further constrains the system by allowing grid electricity to be used exclusively to supplement differences between the separation load and wind electricity availability, while the electrolysis cell is operated solely on wind electricity. This constraint forces the optimization model to prioritize the allocation of renewable energy to the most electricity-intensive process unit.

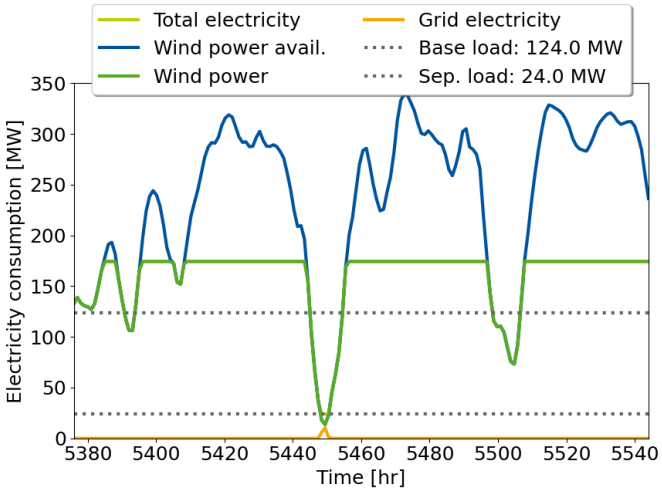

Figure 4: Electricity consumption over time for the CWE case

5.4. Results

The electricity consumption of the first case for an exemplary one week segment can be seen in Figure 2. This approach results in higher CO_2 emissions and higher operating costs due to the fossil-based part of Belgium's grid electricity mix. The static operation does not leverage the potential cost savings or sustainability benefits of renewable energy, making it the least desirable option from both an environmental and economic perspective.

The electricity consumption for the second case, shown in Figure 3, indicates that the steady state load profile without storages and compressors is the best option for the unconstrained case. The optimized process does not ramp up ethylene production to use more of the renewable energy available when wind generation is high. However, it supplements its energy requirements with grid electricity during periods of low wind availability, albeit within the predefined limit of the base load to ensure that renewable energy remains the primary source. This approach achieves a balance between operational continuity and sustainability, resulting in improved renewable energy utilization, negative CO_2 emissions and reduced energy costs.

In the third and constrained case the optimization results, displayed in Figure 4, show a departure from the steady state design. When wind generation is high, the process ramps up ethylene production to the new optimized design capacity, maximizing the use of renewable energy. During periods of low wind availability, the plant draws on its storage and, if necessary, supplements its energy requirements with grid electricity to keep the separation process running. The result is a significant reduction in CO_2 emissions, at the cost of higher capital expenses to account for necessary production adjustments during high and low wind periods. The trade-off between renewable energy utilization and process throughput is critically highlighted in this scenario, demonstrating the model's capability to adapt to stringent renewable energy usage policies.

The simulation results indicate that the time variable optimization approach offers significant benefits. Compared to the baseline SGE scenario total electricity costs are reduced by approximately 23.7% for the VWE and 26.0% for the CWE scenario. Additionally, the percentage of renewable energy of the total energy use, seen in Figure 5, increases to 83.1% and 99.1%, with a renewable capacity utilization of 55.1% and 65.8% respectively. The optimized operations also lead to negative CO_2 emissions of -1.60 $kgCO_2/kgC_2H_4$ and -2.40 $kgCO_2/kgC_2H_4$ in the two renewable integrated cases. These results demonstrate that even with the intermittent nature of wind energy, optimized process design and adaptive process control and scheduling can maintain continuous produc-

tion while enhancing economic and environmental performance.

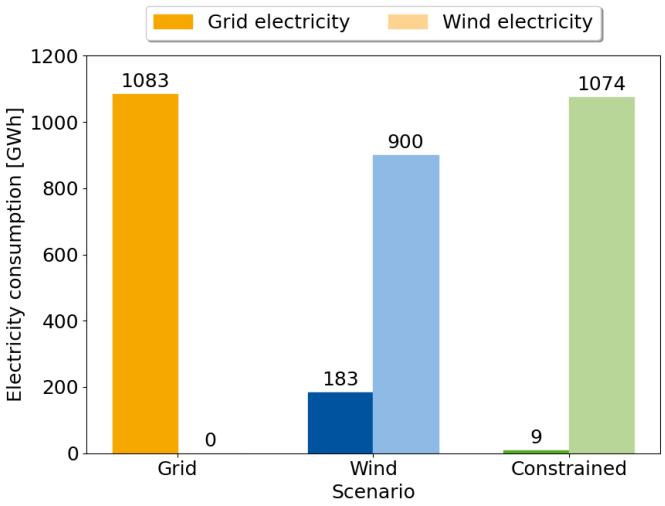

Figure 5: Electricity consumption distribution for the three different cases

This case study highlights how time variable IPPS optimization under intermittent renewable energy supply can significantly enhance process efficiency and sustainability. By effectively integrating renewable energy forecasts, real-time monitoring, and adaptive storage management, the plant maintains robust and flexible operation, dynamically adapting to the inherent variability of renewable resources.

6. Process Performance

In the following section, we evaluate the optimized process in terms of thermodynamic, ecological, and economic performance for all three cases. Then, we compare it with the state of research (SoR) process [20].

6.1. Thermodynamic Evaluation

The thermodynamic performance of the process is evaluated by comparing the electrical energy to the increase in chemical value:

$$\mu_{electric} = \frac{\Delta_r H_{ethylene} \cdot \dot{n}_{ethylene}}{P_{electric}}, \tag{12}$$

where $\mu_{electric}$ is the full process electrical efficiency, $\Delta_r H_{ethylene}$ is the enthalpy of reaction of the CO_2 to ethylene reduction, $\dot{n}_{ethylene}$ is the ethylene product stream, and $P_{electric}$ is the electricity needed to run the process at steady state.

Using this metric, the power necessary to upgrade CO_2 and water in a chemical reaction is 32.3 MW. The electricity duty of our process at steady state is 124 MW. Resulting from these values is a full process electrical efficiency of 26.1 % at steady state. In case 3, the efficiency is lower because intermediary storage induces additional compressor duties.

There is still significant potential to reduce the energy needed in the production of ethylene and, therefore, also in the cost of the final product. The largest contributors to the losses are the low efficiency of the electrolysis cell, the production of unwanted side products, and the high separation duty.

The fully heat integrated process has a specific total energy demand of 192 $MJ/kg_{ethylene}$. Compared to the SoR alkaline electrolysis process by Kim et al. [20] this is a reduction in specific energy demand of 58 %.

6.2. Economic Evaluation

We evaluate the economic feasibility of our process in the three different cases by calculating the net present values (NPVs) and break-even prices (BEPs) for our most important revenue streams and comparing them to the present day market value. The NPV can be calculated using the following formula [81]:

$$\begin{aligned} NPV = &-(C_I + C_W) \\ &+ \sum_{j=1}^{n} (R - X)_j (1 - t_C)/(1 + i_a)^j \\ &+ \sum_{j=1}^{n_t} D_j t/(1 + i_a)^j \\ &+ (C_S + C_W)/(1 + i_a)^n \end{aligned} \tag{13}$$

where:

- C_I: The fixed capital investment or capital expenses
- C_W: The working capital assumed to be $C_W = 0.15 * C_I$
- $(R - X)_j$: The revenue or receipts R minus operational expenses X in year j
- n_t: Depreciation life for tax purposes, assumed to be $n_t = n$
- D_j: The linear depreciation, given as $D_j = (C_I - C_S)/n$
- C_S: The salvage value, assumed to be $C_S = 0.25 * C_I$
- t_C: The corporate tax rate $t_C = 0.25$ [82]

The CAPEX of our process are calculated in ASPEN PLUS®[9] and are scaled depending on the result given by the time variable optimization of each case. The fixed capital investment is then given by the sum of the expenses of all installed units. The yearly operating expenses include the electricity cost including additional compressor duties, the cost of cooling water, the material costs and the cost associated with the treatment of the vented electrolyte. The yearly revenue includes the sale of ethylene and oxygen, CO_2 certificates and heat credits awarded through the burning of our gaseous vent streams.

The NPVs of the three different cases are -1.52, -1.18, and -1.48 billion € respectively. The VWE case has the highest NPV of the three cases as it has lower operational expenses, due to the usage of renewable electricity, while needing no additional capital expenses for storage tanks or an increased electrolysis cell capacity compared to the SGE case. Because all cases have a negative NPV, we can conclude that the technology still needs to be improved before it becomes economically feasible.

To examine under which pricing situations our process would break even we calculated the BEP of our most important revenue streams, the sale of ethylene and the credits awarded through CO_2 certificates. The BEP is the amount of money a product has to be sold at for the NPV to be zero [81].

The BEPs of ethylene for the three cases are shown in Figure 6. Compared to the current market price of 0.827 $€/kg_{C_2H_4}$ [50] an increase of 7-9 times is necessary to reach the BEP. Similarly, the BEPs of CO_2 certificates for the three cases are shown in Figure 7. Here an increase of 18-23 times of the current market price of 100 $€/t_{CO_2}$ [46] is necessary to reach the BEP.

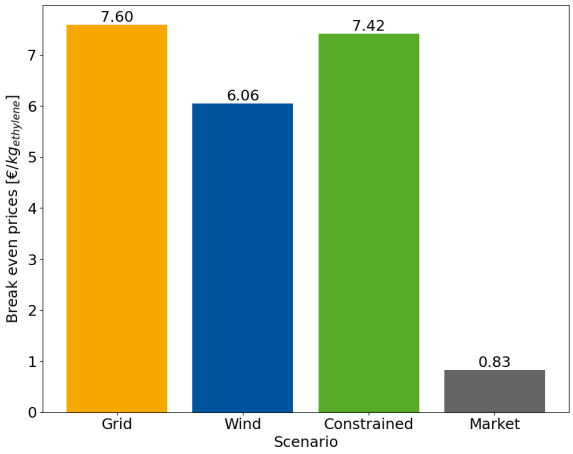

Figure 6: BEP of ethylene in each case compared to current market price

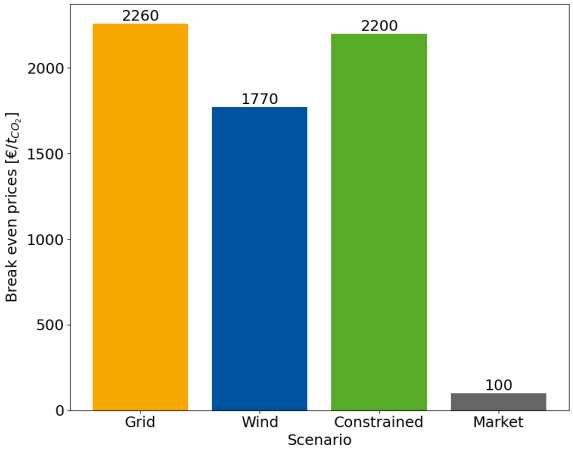

Figure 7: BEP of CO_2 certificates in each case compared to current market price

6.3. Ecological Evaluation

To evaluate the ecological impact of our process, we perform a gate-to-gate life cycle assessment (LCA). A gate-to-gate LCA is chosen because the conditions under which the feed CO_2 is captured are not easily identified. The CO_2 is captured in several power plants and other industrial producers and mixed inside the pipeline. Ethylene can be used in many different products, and therefore we exclude it in the LCA. However, this does mean that a negative value of carbon emissions in this analysis does not automatically transfer to the actual removal of carbon from the atmosphere in the long term. But in comparing the three different cases, the LCA still has value as all cases are calculated using the same metric.

For the LCA, we consider the greenhouse gas (GHG) emissions saved by not emitting the CO_2 to the atmosphere and from all streams exiting the process. Furthermore, we consider GHG emissions by the electricity used in our process. The functional unit is 1 kg of the ethylene product. The entire CO_2 stream entering our process is considered as GHG removed from the atmosphere. Apart from the carbon that ends up in the ethylene product, there are two other possible destinations: it remains unreacted and is vented into the atmosphere, or it is burned in the off-gas and ethanol streams and released as CO_2. Therefore, all CO_2 that is not trapped in the ethylene product is released into the atmosphere again.

The GHG emissions of electricity are split into electricity provided by the grid and electricity from offshore wind. The GHG emissions of grid electricity are estimated

from the current mix of supplied electricity on the Belgian grid: 41.4 % nuclear, 22.3 % fossil gas, 16.6 % wind, 8.8 % hydropower, 7.3 % biomass, and 3.6 % other sources according to the Association of Issuing Bodies [83]. The resulting GHG emissions are 106 kg_{CO_2e}/MWh. Offshore wind power is assumed to have GHG emissions of 13 kg_{CO_2e}/MWh according to the UN Economic Commission for Europe [84]. We attribute all carbon emissions or removal to the ethylene product as it is the primary product of the plant.

Treatment of the electrolyte waste stream, construction, and recycling of the plant are not part of the LCA. Transportation GHG emissions are also neglected in our assessment.

The LCA is performed for all three case studies (see Section 5.3) and the results are compared to the SoR process [20] and ethylene produced by steam cracking [85]. The results for each case are shown in Figure 8:

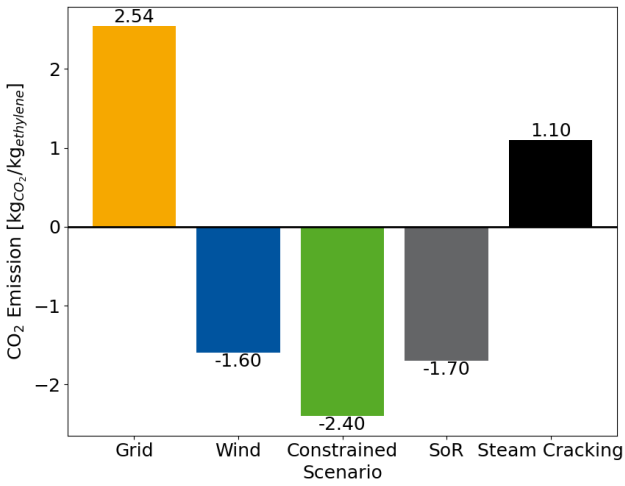

Figure 8: Comparison of CO_2 emissions in each case, SoR, and steam cracking processes

The results vary significantly between each case. This discrepancy can be attributed to the large difference in the source of electricity, since the total amount of ethylene produced is fixed in each case, and the total electricity use is only slightly increased by the additional compressor duty. The grid electricity case study emits 2.5 $kg_{CO_2}/kg_{ethylene}$ which is significantly more than the production of ethylene by steam cracking with 1.1 $kg_{CO_2}/kg_{ethylene}$. In the second case study, due to the use of mostly renewable electricity, there is a removal of 1.6 $kg_{CO_2}/kg_{ethylene}$ from the atmosphere. However, this value is still lower compared the SoR process utilizing only wind power. In the constrained case, where the use of grid electricity is limited to keeping the cryogenic distillation running, the process removes 2.4 $kg_{CO_2}/kg_{ethylene}$ from the atmosphere. This value is significantly better than the current SoR process and shows the potential of our process. One main difference between our case study and the state of research process is incorporating dynamic optimization to improve utilization of renewable electricity.

In case 2 and 3, the cost of CO_2 removal from the atmosphere is 1461 €/Tonne and 1218 €/Tonne, respectively. Although the cost of ethylene is higher in case 3, the cost of CO_2 removal is lower. This is because of the the decrease in grid electricity use and subsequent higher CO_2 removal. However, this value is still higher than the cost of currently operational direct-air capture systems at 500 - 1000 $/Tonne [86].

7. Conclusion

This study presents a novel process for the sustainable production of high-purity ethylene via alkaline electrolysis of captured CO_2, utilizing intermittent renewable electricity. The process is rigorously modeled in ASPEN PLUS®, with integration of renewable energy achieved through a time-variable IPPS optimization in Pyomo.

Environmental performance is evaluated through a gate-to-gate LCA, revealing net-negative GHG emissions of -2.4 $kg_{CO_2}/kg_{ethylene}$. This represents a substantial improvement over both conventional fossil-based and current SoR CO_2-based ethylene production pathways, highlighting the process's strong carbon mitigation potential. Economic viability is assessed using a NPV analysis across different energy scenarios. While the process is not yet cost-competitive under present market conditions, requiring a 7.3-fold increase in ethylene price or a 17.7-fold increase in carbon certificate value, the results indicate clear promise under evolving policy frameworks or future cost reductions in electrolysis and separation technologies.

Post-optimization analysis of the heat-integrated system yields a steady-state electrical efficiency of 26% and a specific energy demand 58% lower than that of the benchmark SoR process. These results underscore the thermodynamic efficiency and resource effectiveness of the proposed design.

Overall, the integration of advanced process modeling with time variable IPPS optimization for renewable energy utilization demonstrates a viable and environmentally beneficial pathway for ethylene production. While economic challenges remain, the process shows strong potential for future implementation, particularly in the context of advancing catalyst technologies and supportive climate policy. This work contributes to the growing foundation for carbon-neutral and fossil-independent chemical manufacturing.

Supplementary Information is attached

References

[1] United Nations, Paris agreement, 2015. URL: https://unfccc.int/sites/default/files/english_paris_agreement.pdf.

[2] World Meteorological Organization, Wmo confirms 2024 as warmest year on record at about 1.55Â°c above pre-industrial level, 01/10/2025. URL: https://wmo.int/news/media-centre/wmo-confirms-2024-warmest-year-record-about-155degc-above-pre-industrial-level.

[3] X. Wang, C. Song, Carbon capture from flue gas and the atmosphere: A perspective, Frontiers in Energy Research 8 (2020).

[4] Y. Wang, Z. Wang, C.-T. Dinh, J. Li, A. Ozden, M. Golam Kibria, A. Seifitokaldani, C.-S. Tan, C. M. Gabardo, M. Luo, H. Zhou, F. Li, Y. Lum, C. McCallum, Y. Xu, M. Liu, A. Proppe, A. Johnston, P. Todorovic, T.-T. Zhuang, D. Sinton, S. O. Kelley, E. H. Sargent, Catalyst synthesis under co2 electroreduction favours faceting and promotes renewable fuels electrosynthesis, Nature Catalysis 3 (2020) 98–106.

[5] S. Ma, M. Sadakiyo, R. Luo, M. Heima, M. Yamauchi, P. J. Kenis, One-step electrosynthesis of ethylene and ethanol from co2 in an alkaline electrolyzer, Journal of Power Sources 301 (2016) 219–228.

[6] S. Sultan, H. Lee, S. Park, M. M. Kim, A. Yoon, H. Choi, T.-H. Kong, Y.-J. Koe, H.-S. Oh, Z. Lee, H. Kim, W. Kim, Y. Kwon, Interface rich cuo/al 2 cuo 4 surface for selective ethylene production from electrochemical co 2 conversion, Energy & Environmental Science 15 (2022) 2397–2409.

[7] A. Alshammari, V. N. Kalevaru, A. Bagabas, A. Martin, Production of ethylene and its commercial importance in the global market, in: J. Davim, H. Al-Megren, T. Xiao (Eds.), Petrochemical Catalyst Materials, Processes, and Emerging Technologies, Advances in Chemical and Materials Engineering, IGI Global, 2016, pp. 82–115. doi:10.4018/978-1-4666-9975-5.ch004.

[8] G. Leonzio, A. Hankin, N. Shah, Co2 electrochemical reduction: A state-of-the-art review with economic and environmental analyses, Chemical Engineering Research and Design 208 (2024) 934–955.

[9] Aspen Technology Inc, Aspen plus v11, 1981-2019.

[10] X. Li, L. Gao, Introduction for integrated process planning and scheduling, in: X. Li, L. Gao (Eds.), Effective Methods for Integrated Process Planning and Scheduling, volume 2 of *Engineering Applications of Computational Methods*, Springer Berlin Heidelberg, Berlin, Heidelberg, 2020, pp. 1–15. doi:10.1007/978-3-662-55305-3{\textunderscore}1.

[11] X. Li, L. Gao (Eds.), Effective Methods for Integrated Process Planning and Scheduling, Engineering Applications of Computational Methods, Springer Berlin Heidelberg, Berlin, Heidelberg, 2020. doi:10.1007/978-3-662-55305-3.

[12] Q. Liu, J. Liu, Z. Dong, M. Zhan, Z. Mei, B. Ying, X. Shao, Integrated optimization of process planning and scheduling for reducing carbon emissions, Journal of Industrial & Management Optimization 17 (2021) 1025–1055.

[13] F. Li, A. Thevenon, A. Rosas-Hernández, Z. Wang, Y. Li, C. M. Gabardo, A. Ozden, C. T. Dinh, J. Li, Y. Wang, J. P. Edwards, Y. Xu, C. McCallum, L. Tao, Z.-Q. Liang, M. Luo, X. Wang, H. Li, C. P. O'Brien, C.-S. Tan, D.-H. Nam, R. Quintero-Bermudez, T.-T. Zhuang, Y. C. Li, Z. Han, R. D. Britt, D. Sinton, T. Agapie, J. C. Peters, E. H. Sargent, Molecular tuning of co2-to-ethylene conversion, Nature 577 (2020) 509–513.

[14] Y. Yao, T. Shi, W. Chen, J. Wu, Y. Fan, Y. Liu, L. Cao, Z. Chen, A surface strategy boosting the ethylene selectivity for co2 reduction and in situ mechanistic insights, Nature communications 15 (2024) 1257.

[15] X. Chen, J. Chen, N. M. Alghoraibi, D. A. Henckel, R. Zhang, U. O. Nwabara, K. E. Madsen, P. J. A. Kenis, S. C. Zimmerman, A. A. Gewirth, Electrochemical co2-to-ethylene conversion on polyamine-incorporated cu electrodes, Nature Catalysis 4 (2021) 20–27.

[16] W. Ma, S. Xie, T. Liu, Q. Fan, J. Ye, F. Sun, Z. Jiang, Q. Zhang, J. Cheng, Y. Wang, Electrocatalytic reduction of co2 to ethylene and ethanol through hydrogen-assisted c–c coupling over fluorine-modified copper, Nature Catalysis 3 (2020) 478–487.

[17] W. Liu, P. Zhai, A. Li, B. Wei, K. Si, Y. Wei, X. Wang, G. Zhu, Q. Chen, X. Gu, R. Zhang, W. Zhou, Y. Gong, Electrochemical co2 reduction to ethylene by ultrathin cuo nanoplate arrays, Nature communications 13 (2022) 1877.

[18] B. Zhang, J. Zhang, M. Hua, Q. Wan, Z. Su, X. Tan, L. Liu, F. Zhang, G. Chen, D. Tan, X. Cheng, B. Han, L. Zheng, G. Mo, Highly electrocatalytic ethylene production from co2 on nanodefective cu nanosheets, Journal of the American Chemical Society 142 (2020) 13606–13613.

[19] C. Choi, S. Kwon, T. Cheng, M. Xu, P. Tieu, C. Lee, J. Cai, H. M. Lee, X. Pan, X. Duan, W. A. Goddard, Y. Huang, Highly active and stable stepped cu surface for enhanced electrochemical co2 reduction to c2h4, Nature Catalysis 3 (2020) 804–812.

[20] T. Kim, P. T. Benavides, Comparative life cycle analysis on ethylene production from electrocatalytic reduction of carbon dioxide, Journal of Cleaner Production 449 (2024) 141348.

[21] M. D. Aminu, S. A. Nabavi, C. A. Rochelle, V. Manovic, A review of developments in carbon dioxide storage, Applied Energy 208 (2017) 1389–1419.

[22] S. Garg, M. Li, A. Z. Weber, L. Ge, L. Li, V. Rudolph, G. Wang, T. E. Rufford, Advances and challenges in electrochemical co 2 reduction processes: an engineering and design perspective looking beyond new catalyst materials, Journal of Materials Chemistry A 8 (2020) 1511–1544.

[23] B. Qin, Y. Li, H. Fu, H. Wang, S. Chen, Z. Liu, F. Peng, Electrochemical reduction of co2 into tunable syngas production by regulating the crystal facets of earth-abundant zn catalyst, ACS applied materials & interfaces 10 (2018) 20530–20539.

[24] K. Wiranarongkorn, K. Eamsiri, Y.-S. Chen, A. Arpornwichanop, A comprehensive review of electrochemical reduction of co2 to methanol: Technical and design aspects, Journal of CO2 Utilization 71 (2023) 102477.

[25] D. Ewis, M. Arsalan, M. Khaled, D. Pant, M. M. Ba-Abbad, A. Amhamed, M. H. El-Naas, Electrochemical reduction of co2 into formate/formic acid: A review of cell design and operation, Separation and Purification Technology 316 (2023) 123811.

[26] X. Chen, Y. Zhao, J. Han, Y. Bu, Copper-based catalysts for electrochemical reduction of carbon dioxide to ethylene, ChemPlusChem 88 (2023) e202200370.

[27] M. Li, B. Hua, L.-C. Wang, J. D. Sugar, W. Wu, Y. Ding, J. Li, D. Ding, Switching of metal–oxygen hybridization for selective co2 electrohydrogenation under mild temperature and pressure, Nature Catalysis 4 (2021) 274–283.

[28] Global Industry Analysis Inc, Ethylene - global strategic business report, 2025. URL: https://www.researchandmarkets.com/reports/354876/ethylene_global_strategic_business_report.

[29] M. Jouny, G. S. Hutchings, F. Jiao, Carbon monoxide electroreduction as an emerging platform for carbon utilization, Nature Catalysis 2 (2019) 1062–1070.

[30] W. Ni, H. Chen, N. Tang, T. Hu, W. Zhang, Y. Zhang, S. Zhang, High-purity ethylene production via indirect carbon dioxide electrochemical reduction, Nature communications 15 (2024) 6078.

[31] M. Holst, S. Aschbrenner, T. Smolinka, C. Voglstätter, G. Grimm, :unav, Cost forecast for low temperature electrolysis - technology driven bottom-up prognosis for pem and alkaline water electrolysis systems, 2020. doi:10.24406/publica-1318.

[32] Q. Ding, Z. Zhang, P. Zhang, C. Yu, C.-H. He, X. Cui, H. Xing, One-step ethylene purification from ternary mixture by synergetic molecular shape and size matching in a honeycomb-like ultramicroporous material, Chemical Engineering Journal 450 (2022) 138272.

[33] B. Zhu, J.-W. Cao, S. Mukherjee, T. Pham, T. Zhang, T. Wang, X. Jiang, K. A. Forrest, M. J. Zaworotko, K.-J. Chen, Pore engineering for one-step ethylene purification from a three-component hydrocarbon mixture, Journal of the American Chemical Society 143 (2021) 1485–1492.

[34] X. Cui, K. Chen, H. Xing, Q. Yang, R. Krishna, Z. Bao, H. Wu, W. Zhou, X. Dong, Y. Han, B. Li, Q. Ren, M. J. Zaworotko, B. Chen, Pore chemistry and size control in hybrid porous materials for acetylene capture from ethylene, Science (New York, N.Y.) 353 (2016) 141–144.

[35] S. Mukherjee, D. Sensharma, K.-J. Chen, M. J. Zaworotko, Crystal engineering of porous coordination networks to enable separation of c2 hydrocarbons, Chemical communications (Cambridge, England) 56 (2020) 10419–10441.

[36] P.-Q. Liao, W.-X. Zhang, J.-P. Zhang, X.-M. Chen, Efficient purification of ethene by an ethane-trapping metal-organic framework, Nature communications 6 (2015) 8697.

[37] T. He, Y. Xiao, Q. Zhao, M. Zhou, G. He, Ultramicroporous metal–organic framework qc-5-cu for highly selective adsorption of co 2 from c 2 h 4 stream, Industrial & Engineering Chemistry Research

59 (2020) 3153–3161.
[38] J.-W. Cao, S. Mukherjee, T. Pham, Y. Wang, T. Wang, T. Zhang, X. Jiang, H.-J. Tang, K. A. Forrest, B. Space, M. J. Zaworotko, K.-J. Chen, One-step ethylene production from a four-component gas mixture by a single physisorbent, Nature communications 12 (2021) 6507.
[39] V. Carravetta, A. H. d. A. Gomes, R. D. R. T. Marinho, G. Öhrwall, H. Ågren, O. Björneholm, A. N. de Brito, An atomistic explanation of the ethanol-water azeotrope, Physical chemistry chemical physics : PCCP 24 (2022) 26037–26045.
[40] Cameo Chemicals, Potassium hydroxide, [dry solid, flake, bead, or granular]: Chemical datasheet - physical properties, 2024. URL: https://cameochemicals.noaa.gov/chemical/9484.
[41] C. A. European Commision, Climate action progress report 2023: Country profile - belgium, 2024. URL: https://climate.ec.europa.eu/document/download/78cf1df3-339c-4d93-949b-41e041016177_en?filename=be_2023_factsheet_en.pdf.
[42] A. Ingvarsdóttir, Comparison of direct air capture technology to point source co2 capture in iceland, 2020. URL: https://www.diva-portal.org/smash/get/diva2:1520216/FULLTEXT01.pdf.
[43] Fluxys Belgium SA, Co_2: Preparing to build the network, 2025. URL: https://www.fluxys.com/en/projects/carbon-preparing-to-build-the-network.
[44] Fluxys Belgium SA, Carbon specification proposal, 2022.
[45] European Union, Consolidated text: Directive 2003/87/ec of the european parliament and of the council of 13 october 2003 establishing a system for greenhouse gas emission allowance trading within the union and amending council directive 96/61/ec, 2024. URL: http://data.europa.eu/eli/dir/2003/87/2024-03-01.
[46] FPS Public Health, Food Chain Safety and Environment, Carbon pricing - main results, 2024. URL: https://climat.be/2050-en/carbon-pricing/main-results.
[47] ARG mbH & Co. KG, Arg ethylene pipeline, 2025. URL: https://argkg.com.
[48] BASF, Basf antwerp, 2025. URL: https://www.basf.com/be/en/who-we-are/Group-Companies/BASF-Antwerpen.
[49] Argus media group, Argus ethylene and derivatives methodology, 2025.
[50] I. Statista, Price of ethylene worldwide from 2017 to 2023, 2024. URL: https://www.statista.com/statistics/1170573/price-ethylene-forecast-globally/.
[51] S. Nitopi, E. Bertheussen, S. B. Scott, X. Liu, A. K. Engstfeld, S. Horch, B. Seger, I. E. L. Stephens, K. Chan, C. Hahn, J. K. Nørskov, T. F. Jaramillo, I. Chorkendorff, Progress and perspectives of electrochemical co2 reduction on copper in aqueous electrolyte, Chemical reviews 119 (2019) 7610–7672.
[52] International Energy Agency, Belgium: Electricity, 2024. URL: https://www.iea.org/countries/belgium/electricity.
[53] Belgian Offshore Platform, Projects, 2025. URL: https://www.belgianoffshoreplatform.be/en/projects/.
[54] Elia Group, The princess elisabeth island, 2025. URL: https://www.elia.be/en/infrastructure-and-projects/infrastructure-projects/princess-elisabeth-island.
[55] European Investment Bank, Princess elisabeth zone lot 1 offshore wind farm, 2025. URL: https://www.eib.org/de/projects/pipelines/all/20240726.
[56] FPS Economy, Summary of tender principles for the princess elisabeth zone, 2023. URL: https://economie.fgov.be/sites/default/files/Files/Energy/Tender-principles-Princess-Elisabeth-Zone.pdf.
[57] F. Trepte, pwc, Power purchase agreements (ppa): Securing green electricity for the long term, 2025. URL: https://www.pwc.de/en/energy-sector/renewable-energy/power-purchase-agreements-ppa.html.
[58] International Energy Agency, Levelised cost of electricity calculator, 2020. URL: https://www.iea.org/data-and-statistics/data-tools/levelised-cost-of-electricity-calculator.
[59] The European Chemical Industry Councel, AISBL, A pillar of the european economy: Landscape of the european chemical industry - belgium, 2024. URL: https://cefic.org/a-pillar-of-the-european-economy/landscape-of-the-european-chemical-industry/belgium/.
[60] Mechanical Business, Refrigeration - achieving ultra-low temperatures, 2021. URL: https://issuu.com/mechbusiness/docs/mb02.21lr/s/11701713.
[61] TLK Energy GmbH, Pinch analysis online, 2025. URL: https://tlk-energy.de/en/tools/pinch-analysis-online.
[62] M. H. Rashid (Ed.), Electric renewable energy systems, Elsevier/AP Academic Press is an imprint of Elsevier, Amsterdam, 2016.
[63] K. Mongird, V. Fotedar, V. Viswanathan, V. Koritarov, P. Balducci, B. Hadjerioua, J. Alam, Energy storage technology and cost characterization report, 2019. URL: https://www.energy.gov/sites/default/files/2019/07/f65/Storage%20Cost%20and%20Performance%20Characterization%20Report_Final.pdf.
[64] The University of Texas at Austin, Capital expenditures, 2025. URL: https://energy.utexas.edu/policy/fce/framework/capital-expenditures.
[65] B. Zohuri, Hybrid Energy Systems, Springer International Publishing, Cham, 2018. doi:10.1007/978-3-319-70721-1.
[66] Z. Gao, S. Sheng, Real-time monitoring, prognosis, and resilient control for wind turbine systems, Renewable Energy 116 (2018) 1–4.
[67] K. Roh, L. C. Brée, K. Perrey, A. Bulan, A. Mitsos, Flexible operation of switchable chlor-alkali electrolysis for demand side management, Applied Energy 255 (2019) 113880.
[68] C. G. Edge, V. Irvine, A Practical Approach to the Appraisal of Capital Expenditures, 2 ed., Society of Management Accountants of Canada, Hamilton, 1981.
[69] R. H. Perry, D. W. Green, Perry's chemical engineers' handbook, 8th ed. ed., McGraw-Hill, New York, 2008.
[70] J. C. Butcher, Numerical methods for ordinary differential equations, J. Wiley, Chichester West Sussex England and Hoboken NJ, 2003.
[71] W. E. Hart, J.-P. Watson, D. L. Woodruff, Pyomo: modeling and solving mathematical programs in python, Mathematical Programming Computation 3 (2011) 219–260.
[72] M. L. Bynum, G. A. Hackebeil, W. E. Hart, C. D. Laird, B. L. Nicholson, J. D. Siirola, J.-P. Watson, D. L. Woodruff, Pyomo — Optimization Modeling in Python, volume 67, Springer International Publishing, Cham, 2021. doi:10.1007/978-3-030-68928-5.
[73] A. Wächter, L. T. Biegler, On the implementation of an interior-point filter line-search algorithm for large-scale nonlinear programming, Mathematical Programming 106 (2006) 25–57.
[74] Fraunhofer ISE, Electricity production and spot prices in belgium in 2019, 2025. URL: https://energy-charts.info/charts/price_spot_market/chart.htm?l=en&c=BE&stacking=stacked_absolute_area&legendItems=8y6&interval=year&year=2019.
[75] ENTSO-E, Market energy prices, 2015. URL: https://newtransparency.entsoe.eu/market/energyPrices.
[76] E. European Commission, Electricity prices for non-household consumers - bi-annual data (from 2007 onwards), 2025. URL: https://ec.europa.eu/eurostat/databrowser/view/nrg_pc_205__custom_15889752/default/table?lang=en.
[77] S. Pfenninger, I. Staffell, Long-term patterns of european pv output using 30 years of validated hourly reanalysis and satellite data, Energy 114 (2016) 1251–1265.
[78] I. Staffell, S. Pfenninger, Using bias-corrected reanalysis to simulate current and future wind power output, Energy 114 (2016) 1224–1239.
[79] S. Pfenninger, Staffell I., Renewables.ninja, 2016. URL: https://www.renewables.ninja/.
[80] M. M. Rienecker, M. J. Suarez, R. Gelaro, R. Todling, J. Bacmeister, E. Liu, M. G. Bosilovich, S. D. Schubert, L. Takacs, G.-K. Kim, S. Bloom, J. Chen, D. Collins, A. Conaty, A. Da Silva, W. Gu, J. Joiner, R. D. Koster, R. Lucchesi, A. Molod, T. Owens, S. Pawson, P. Pegion, C. R. Redder, R. Reichle, F. R. Robertson, A. G. Ruddick, M. Sienkiewicz, J. Woollen, Merra: Nasa's modern-era retrospective analysis for research and applications, Journal of Climate 24 (2011) 3624–3648.
[81] L. T. Biegler, Systematic methods of chemical process design, Prentice Hall international series in the physical and chemical engineering sciences, Prentice Hall PTR, Upper Saddle River, N.J., 1997.
[82] C. Zenner, Belgium - corporate - taxes on corporate income, 2025. URL: https://taxsummaries.pwc.com/belgium/corporate/taxes-on-corporate-income.
[83] Association of Issuing Bodies, European residual mixes 2023: Results of the calculation of residual mixes for the calender year 2023, 2024. URL: https://www.aib-net.org/sites/default/files/assets/facts/residual-mix/2023/AIB_2023_Residual_Mix_FINALResults0907 2024.pdf.
[84] UNITED NATIONS ECONOMIC COMMISSION FOR EUROPE, Carbon neutrality in the unece region: Integrated life-cycle assessment of electricity sources, 2022. URL: https://unece.org/sites/default/files/2022-04/LCA_3_FINAL%20March%202022.pdf.
[85] O. Mynko, I. Amghizar, D. J. Brown, L. Chen, G. B. Marin, R. F. de Alvarenga, D. C. Uslu, J. Dewulf, K. M. van Geem, Reducing co2 emissions of existing ethylene plants: Evaluation of different revamp strategies to reduce global co2 emission by 100 million tonnes, Journal of Cleaner Production 362 (2022) 132127.
[86] P. de Luna, Will direct air capture ever cost less than $100 per ton of co_2?, Forbes (11/29/2024).